Publications of the Astronomical Society of Australia (PASA), Vol. 30, e026, 11 pages.

doi:10.1017/pas.2013.001

GSC 4019 3345: An A-Type Twin Binary

V. Bakış[1,2], H. Bakış[1] and Z. Eker[1]

[1]Department of Space Sciences and Technologies, Akdeniz University Science Faculty, Antalya, Turkey
[2]Corresponding author. Email: volkanbakis@akdeniz.edu.tr

(Received October 18, 2012; Accepted January 9, 2013; Online Publication March 1, 2013)

Abstract

Physical dimensions and evolutionary status of the A-type twin binary GSC 4019 3345 are presented. Located at a distance of ∼1.1 kpc from the Sun, the system was found to have two components with identical masses ($M_{1,2} = 1.92$ M$_\odot$), radii ($R_{1,2} = 1.76$ R$_\odot$), and luminosities (log $L_{1,2} = 1.1$ L$_\odot$) revolving in a circular orbit. Modeling the components with theoretical evolutionary tracks and isochrones implies a young age ($t = 280$ Myr) for the system, which is bigger than the synchronization time scale but smaller than the circularization time scale. Nevertheless, synthetic spectrum models revealed components' rotation velocity of $V_{\rm rot12} = 70$ km s^{-1}, that is about three times higher than their synchronization velocity. No evidence is found for an age difference between the components.

Keywords: binaries: close – binaries: twins – binaries: spectroscopic – eclipses

1 INTRODUCTION

Statistical studies on the mass ratio distribution of binaries (e.g. Lucy 2006; Simon & Obbie 2009) showed that the frequency of existing twins within the mass ratio 0.98–1.00 is about 3% among all binaries, at which F, G, and K spectral type systems dominate. The sample list of twins studied by Simon & Obbie (2009) consisted of 1 O-type, 1 B-type, 3 A-type, 16 F-type, 11 G-type, and 3 K-type twins. This result enabled Simon & Obbie to suggest that low-mass twins are formed in binary populations in which the accretion processes have the time to proceed to completion. Therefore, the discovery of additional twins of earlier spectral types is important statistically for understanding binary formation mechanisms. The existence of early-type twins also suggested that the formation of binaries with components more massive than 1.6 M$_\odot$ might be similar to those for the less massive ones (Zinnecker & Yorke 2007) but other mechanisms might also be important (Simon & Obbie).

In order to test whether late- and early-type systems have the same formation mechanisms, precise observations and detailed analysis of early-type twins especially the eclipsing ones are of special interest. Eclipsing twins are also important astrophysically since they provide the highest precision astrophysical parameters among the others.

In this paper, we studied the recently discovered twin eclipsing binary GSC 4019 3345, which is relatively faint (V∼12 mag) and relatively long period ($P_{\rm orb} = 4.08$ days) among the common eclipsing systems. Its photometric variability has been discovered by Bakış et al. (2007) and twin nature of the binary system is concluded in this paper. Since its discovery, systematic photometry and spectroscopy have been performed to determine the precise orbital period and also to test whether or not the two minima in the preliminary light curve (LC) are precisely equal. Nevertheless, measured times of minima have shown that the published period of $P_{\rm orb} = 4.077278$ days is true with a small update (Section 2.2) and constant with an accuracy of 3×10^{-6} days. Component masses are same within an accuracy of 0.1%.

2 OBSERVATIONS

2.1 Photometry

Photometry of GSC 4019 3345 ($\alpha = 00^{\rm h}22^{\rm m}45\overset{\rm s}{.}37$, $\delta = 62°20'05''.5$) has been carried out in 2004, 2005, 2006, 2007, and 2009 observing seasons. Observations between 2004 and 2007 are mainly based on the time of minimum observations using several telescopes (0.3- and 0.4-m Cassegrain–Schmidt) and CCD cameras (SBIG ST10XME and SBIG ST1001E) of the Çanakkale Onsekiz Mart University Observatory (COMUO) in order to determine the precise orbital period of the binary system. Only Johnson V-band data were studied due to its higher quality with respect to other filters used during the observations between 2004 and 2007. After determining the accurate orbital period of the system, a 1.22-m telescope of COMUO equipped with ST1001E

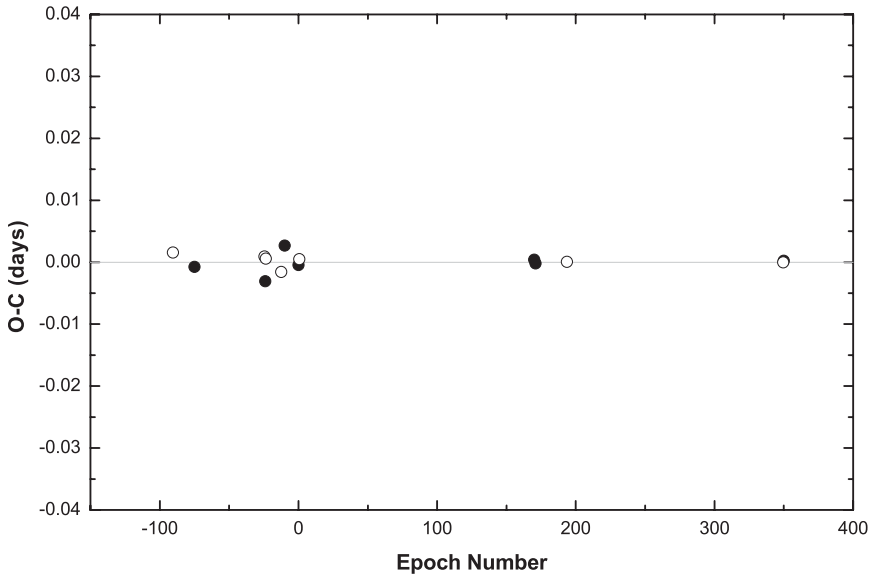

Figure 1. $O - C$ diagram of GSC 4019 3345. Filled and empty circles are from primary and secondary times of minima, respectively.

Table 1. Log of photometric observations of GSC 4019 3345.

Day	Filter	Number of exposures
30.09.2004	*UBVR*	222
27.11.2004	*UBVR*	79
02.12.2004	*UBVR*	132
26.06.2005	*UBVR*	144
28.06.2005	*UBVR*	62
30.06.2005	*UBVR*	110
14.08.2005	*UBVR*	57
24.08.2005	*UBVR*	52
20.09.2005	*BVR*	35
04.10.2005	*BVR*	28
06.10.2005	*BVR*	109
21.10.2005	*BVR*	57
26.10.2005	*BVR*	50
28.08.2007	*BVRI*	145
31.08.2007	*BVRI*	187
01.09.2007	*BVRI*	79
06.09.2007	*BVRI*	122
02.12.2007	*BVRI*	102
20.08.2009	*UBVRI*	43
23.08.2009	*UBVRI*	33
25.08.2009	*UBVRI*	35
29.08.2009	*UBVRI*	47
30.08.2009	*UBVRI*	38
31.08.2009	*UBVRI*	32
03.09.2009	*UBVRI*	38
13.09.2009	*UBVRI*	28
19.09.2009	*UBVRI*	16
23.09.2009	*UBVRI*	45
26.09.2009	*UBVRI*	42
28.09.2009	*UBVRI*	39
29.09.2009	*UBVRI*	39
05.10.2009	*UBVRI*	53
06.10.2009	*UBVRI*	50

Table 2. Times of minimum of GSC 4019 3345.

No.	HJD (−240 0000)	Error	Type (pri/sec)	$O - C$ (days)
1	53279.2902	8	sec	0.0016
2	53342.4861	11	pri	−0.0008
3	53548.3917	7	sec	0.0009
4	53550.4263	13	pri	−0.0031
5	53552.4686	6	sec	0.0006
6	53597.3168	11	sec	−0.0016
7	53607.5143	11	pri	0.0027
8	53648.2842	6	pri	−0.0005
9	53650.3227	4	sec	−0.0006
10	54341.4268	4	pri	0.0004
11	54345.5035	7	pri	−0.0002
12	54437.2431	1	sec	0.0001
13	55073.3025	3	sec	0.0000
14	55075.3414	6	pri	0.0002

CCD has been used in the 2009 observing season to obtain the whole light curve in *UBVR* and *I*-band filters. A total of 15 nights were allocated for the CCD photometry of the system. For differential photometry, GSC 4019 2747 ($\alpha = 00^{\rm h}22^{\rm m}42\overset{\rm s}{.}97$, $\delta = 62°18'35''.3$, $V{\sim}11.4$ mag) and GSC 4019 2784 ($\alpha = 00^{\rm h}22^{\rm m}17\overset{\rm s}{.}97$, $\delta = 62°21'33''.7$, $V{\sim}11.7$ mag) were chosen for comparison and as a check star, respectively. The average standard deviations of a typical observation in *UBVR* and *I* bands are $\sigma = 0.058$, 0.009, 0.008, 0.008 and 0.009, respectively. The log of photometric observations is given in Table 1.

The reduction of CCD frames was made by means of the aperture photometry with C-Muniwin[1] package, on which one of the authors has development contribution. The

[1] http://c-munipack.sourceforge.net/

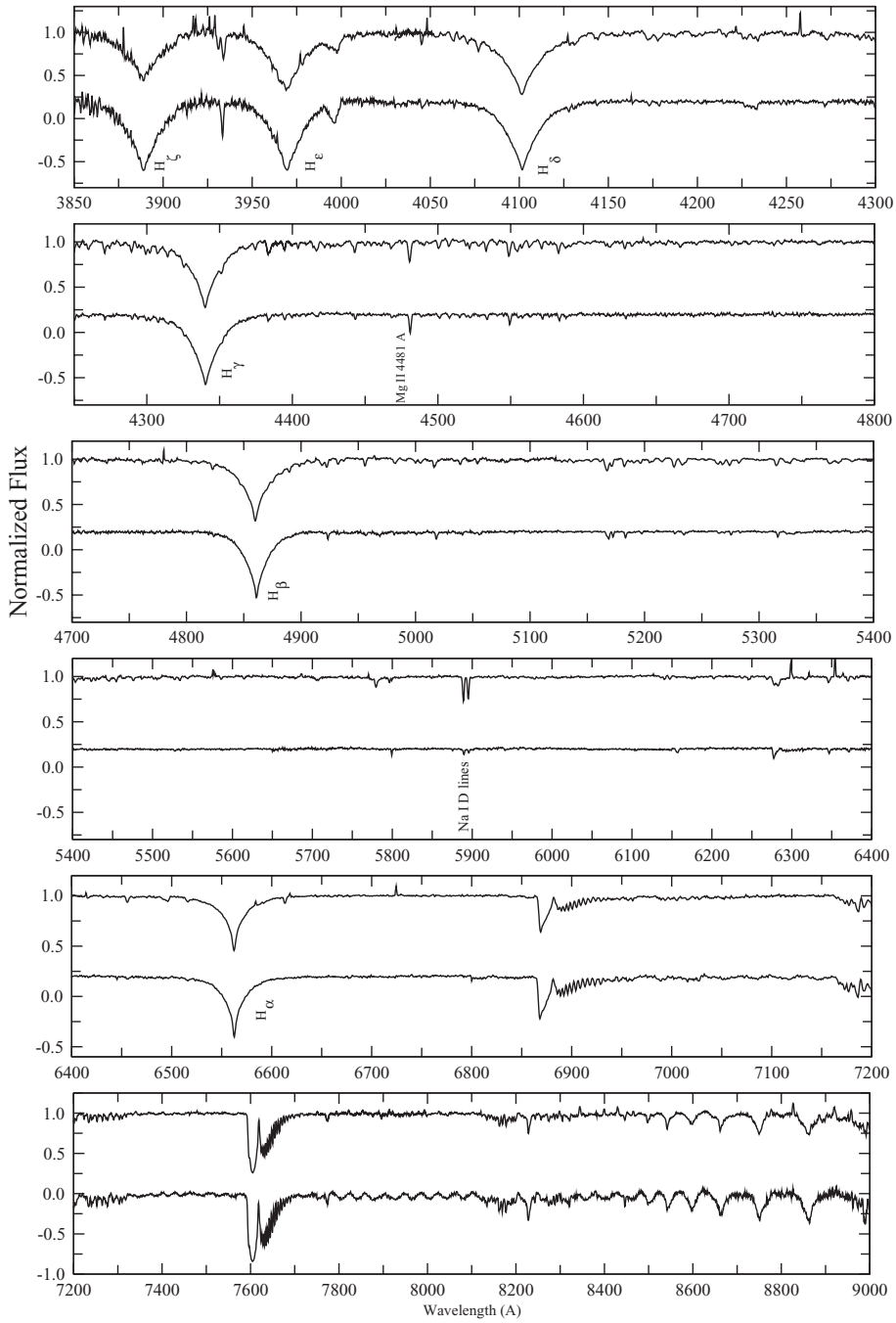

Figure 2. Observed spectrum of GSC 4019 3345 (at $\phi = 0.5$) (upper) and Vega (lower).

reduction of CCD frames is standard: bias and dark subtraction and flat field correction. The size of apertures during the computation of magnitudes of stars in the CCD field selected was about three times the Full Width at Half Maximum (FWHM) of the star profile so that no flux is lost and noise has no considerable effect. The airmass for program stars has not been taken into account due to their proximity with less than 7 arcmin in the sky.

The B and V magnitudes of stars in the same CCD field of GSC 4019 3345 are available in several survey catalogs (i.e. Tycho-2, Høg et al. 2000; United States Naval Observatory (USNO), Monet et al. 1997). Using these catalog magnitudes of stars, we standardized B and V magnitudes of GSC 4019 3345 at light maximum as $B = 12.55(0.10)$ and $V = 12.15(0.02)$.

2.2 Orbital period

A total of 14 times of minima are extracted from the photometric observations of the system between 2004 and 2009.

Table 3. Journal of spectroscopic observations for GSC 4019 3345. S/N refers to the continuum near 6 500 Å.

No	HJD (−240 0000)	Exp. time (s)	S/N	Phase (ϕ)	RV_1 (km s^{-1})	$(O-C)_1$ (km s^{-1})	RV_2 (km s^{-1})	$(O-C)_2$ (km s^{-1})
1	55455.2941	1 800	70	0.187	−92.9	2.5	94.1	−2.1
2	55455.3204	1 800	120	0.194	−90.9	5.8	96.2	−1.4
3	55455.5186	1 800	30	0.242	−103.3	−0.9	97.3	−6.0
4	55456.3890	1 800	110	0.456	−36.3	−5.7	31.7	0.9
5	55456.4303	1 800	130	0.466	−31.7	−8.7	29.4	6.3
6	55456.4524	1 800	110	0.471	−36.0	−16.8	20.7	1.4
7	55456.5594	1 800	130	0.497	−7.2	−3.7	–	–
8	55456.5813	1 800	72	0.503	−5.3	−5.8	–	–
9	55457.2650	1 800	50	0.671	98.2	5.3	−90.1	3.7
10	55457.2905	1 800	60	0.677	92.3	−2.5	−94.2	1.5
11	55457.3824	1 800	50	0.699	98.1	−2.8	−100.0	1.9
12	55457.5735	1 800	50	0.746	104.0	−1.9	−105.9	1.1
13	55457.5922	1 800	50	0.751	104.0	−1.9	−105.9	1.0
14	55795.2997	1 200	50	0.577	47.0	−3.5	−48.9	2.1
15	55795.3166	1 200	50	0.581	49.4	−1.1	−51.3	−0.2
16	55795.3558	1 200	30	0.591	54.8	−2.7	−56.7	1.4
17	55795.3726	1 200	40	0.595	57.0	−0.5	−58.9	−0.8
18	55795.3900	1 200	45	0.599	59.3	−1.6	−61.2	0.3
19	55795.5144	1 200	40	0.630	74.4	−1.5	−76.3	0.3
20	55795.5307	1 200	40	0.634	76.2	−2.5	−78.1	1.4
21	55795.5472	1 200	35	0.638	77.9	−0.7	−79.8	−0.4
22	55795.5933	1 200	28	0.649	82.6	−1.3	−84.5	0.3
23	55863.2090	1 800	85	0.232	−105.5	−3.8	103.6	0.9
24	55863.2343	1 800	75	0.239	−105.8	−3.7	103.9	0.9
25	55863.2598	1 800	50	0.245	−110.6	−8.3	109.9	6.6
26	55863.3449	1 800	120	0.266	−105.2	−3.4	106.3	3.5
27	55863.3693	1 800	70	0.272	−99.2	2.1	101.9	−0.4
28	55863.4491	1 800	60	0.291	−101.9	−2.8	100.0	0.0

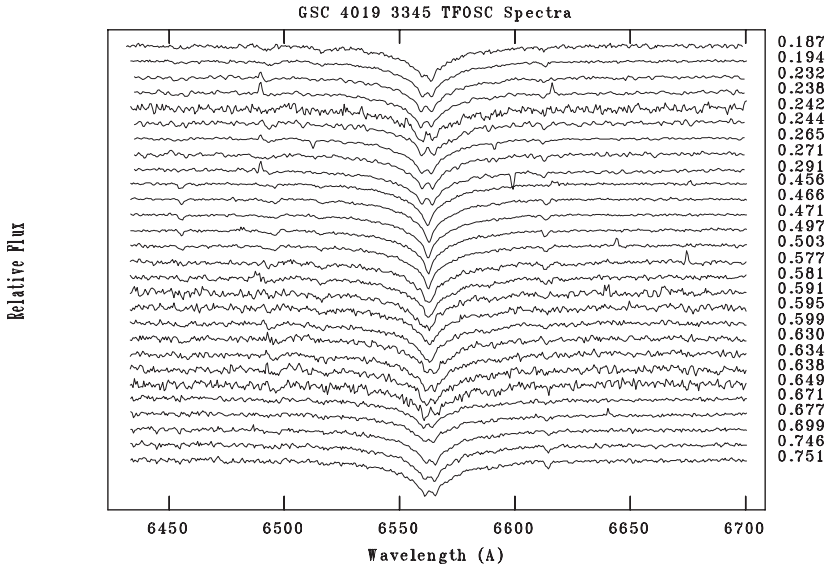

Figure 3. The Hα (6 563 Å) lines of the components of GSC 4019 3345. Orbital phases are shown on the right.

The method described by Kwee & van Woerden (1956) was used for the determination of times of minima. The times of minima extracted are listed in Table 2 together with their uncertainties and minimum types. The regression analysis of the $O-C$ data (for the observing span from 2004 to 2009) improved the orbital period $P_{\rm orb} = 4.077278$ days given by Bakış et al. (2007) and provided the new ephemeris:

$$\text{Pri HJD} = 245\,3648.2847(4) + 4.077304(3) \times E. \quad (1)$$

Based on the new ephemeris (Equation (1)), the calculated $O-C$ values are also included in Table 2. The $O-C$

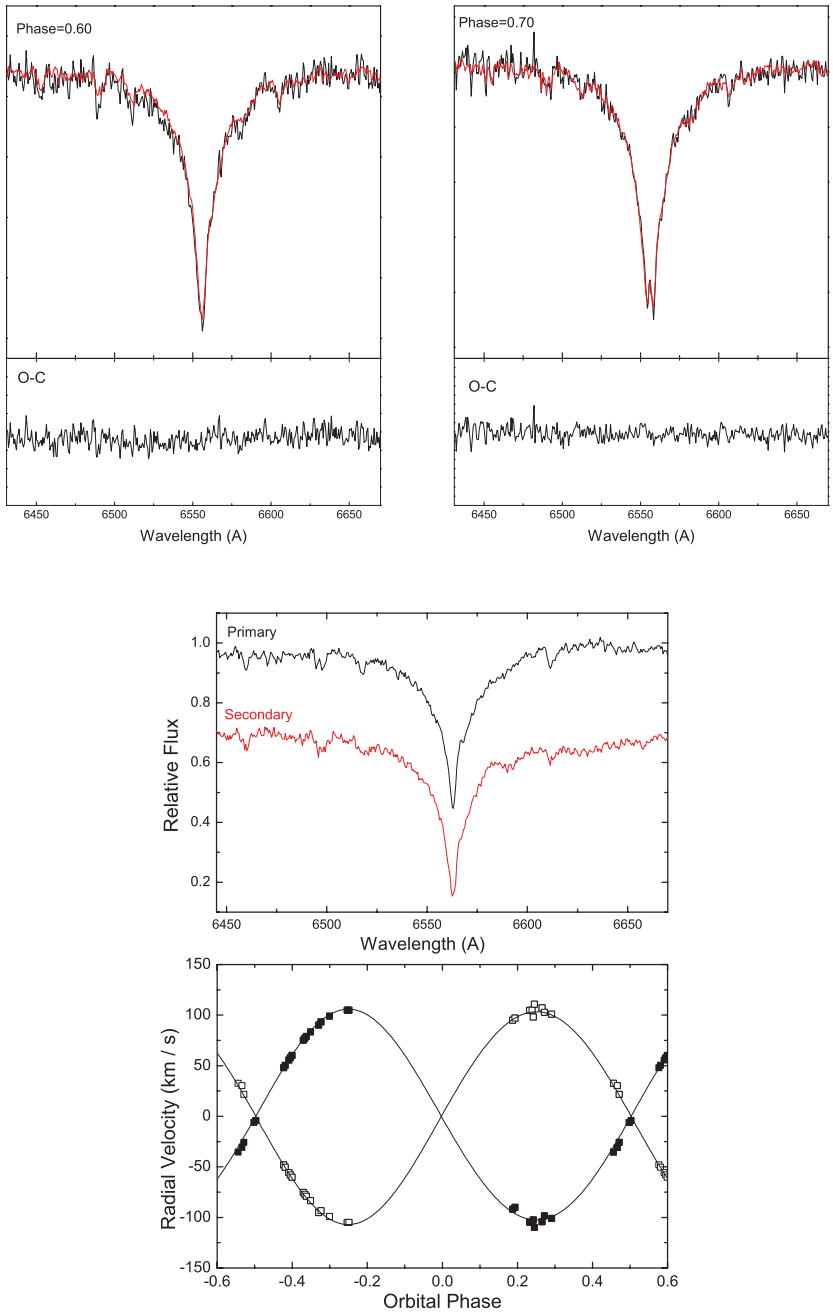

Figure 4. Top: spectral disentangling results on selected spectra around Hα. Observations and fits are shown in black and red, respectively. Middle: reconstructed spectrum of the components. Bottom: best-fitting orbital solution, where filled and empty squares are of primary and secondary RVs, respectively.

diagram is shown in Figure 1, where the consistency of the orbital period is clear with an accuracy better than 3×10^{-6} days.

2.3 Spectroscopy

The spectra of GSC 4019 3345 were taken with the Faint Object Spectrograph and Camera (TFOSC) of the TUBITAK National Observatory (TUG), Turkey. It is attached on the Cassegrain focus of the 1.5-m telescope called RTT150 located at Bakırlıtepe (~36°49^m N, 30°20^m E; altitude = 2 500 m), Antalya. TFOSC has two main capabilities: (a) direct imaging and (b) low-/medium-resolution spectroscopy, both operated by a Linux operating system. For imaging and spectroscopy the same CCD, which has a field of view of 13.3 × 13.3 arcmin with a chip dimension of 2 048 × 2 048 pixels with a pixel size 15 × 15 μm, is used. The spectrograph

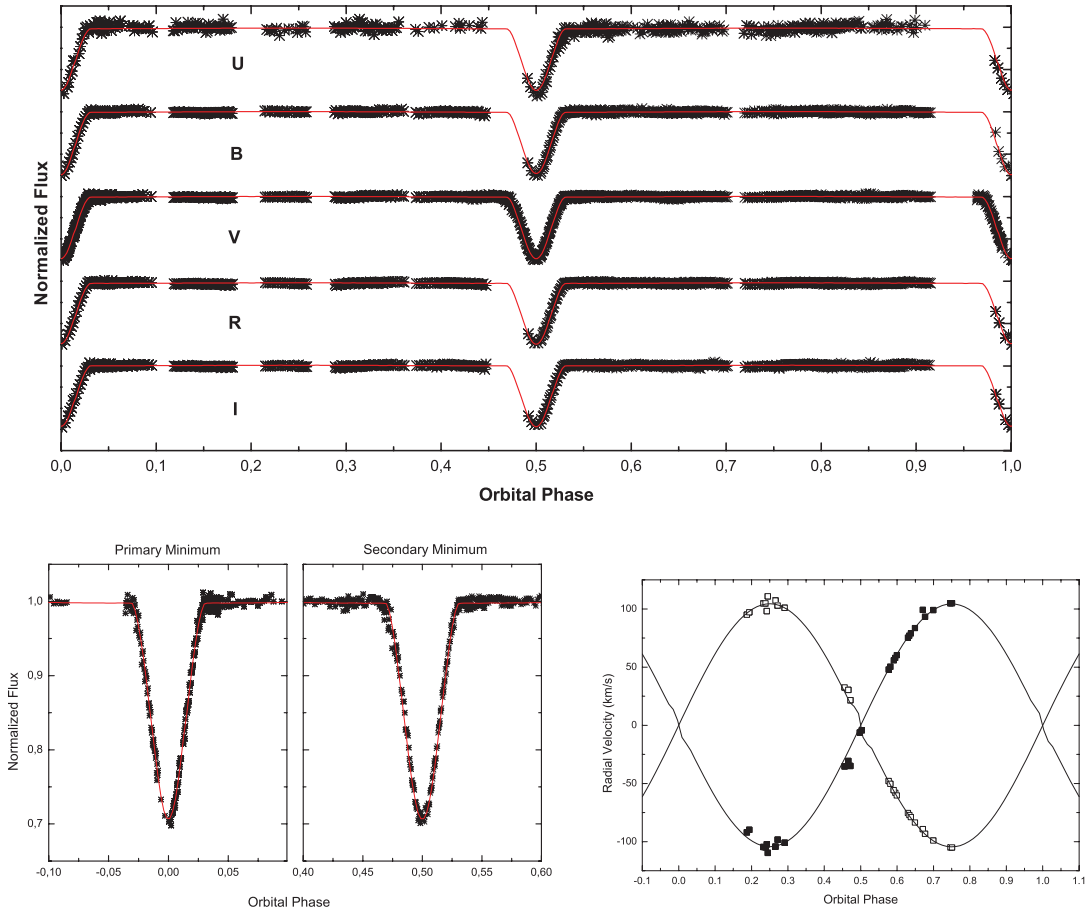

Figure 5. Top: best-fitting LC models in *UBVR* and *I* bands. Lower left: primary and secondary minima with theoretical fit. Lower right: RV curves of the components together with the theoretical model; filled and empty squares are for primary and secondary components, respectively.

was designed to provide a continuous wavelength coverage between 330 and 1 200 nm and has a resolution range of $R(\lambda/\delta\lambda)\sim$205–5 099 with a different wavelength interval. The grisms are used to change the resolutions. The list of available grisms and the resulting resolutions is given in the instrument's manual.[2]

In this project, we have chosen the highest available resolution mode ($R\sim$5 099) of TFOSC, which provides a continuous wavelength coverage of 330–900 nm in 11 échelle orders. All spectra presented in this paper are obtained in three observing sessions (2010 September, 2011 August, and 2011 October). The total number of spectra obtained for GSC 4019 3345 is 28. We have observed radial velocity (RV) standard star Vega (α Lyrae) in each observing night in order to standardize our RV measurements.

Comparison spectra of the iron–argon arc lamp for the wavelength calibration were recorded before and after each exposure. For the exact time of the stellar observation, the dispersion solution was interpolated between the two spectra of the arc lamp. A set of white lamp images was taken every night for flat-fielding.

Table 4. Spectroscopic orbital parameters of GSC 4019 3345.

Parameter	Value
P (days)	4.077304
T_0(HJD − 245 0000)	3 648.2846 ± 0.0001
K_1 (km s^{-1})	105.0 ± 0.8
K_2 (km s^{-1})	105.1 ± 0.8
e	0.03 ± 0.01
w (°)	273 ± 16
V_γ (km s^{-1})	−0.80 ± 1.30
q	1.00 ± 0.01
rms (km s^{-1})	2.8

All spectra were reduced with the Image Reduction and Analysis Software (IRAF).[3] The reduction is standard for échelle spectra: bias subtraction, scattered light correction, aperture extraction, flat-field correction, and dispersion solution for wavelength calibration.

An observed sample spectrum at phase $\phi\sim0.5$ of GSC 4019 3345 and of Vega (α Lyr) with the same instrument is

[2] http://www.tug.tubitak.gov.tr/rtt150_tfosc.php

[3] IRAF is distributed by the National Optical Astronomy Observatories, which are operated by the Association of Universities for Research in Astronomy Inc., under cooperative agreement with the National Science Foundation.

Table 5. Results from the simultaneous solution of *UBVR* and *I*-band LCs and RVs. Adjusted and fixed parameters are presented in separate panels of the table. Uncertainties of adjusted parameters are given in parentheses.

Parameter	Symbol	Value
Adjusted parameters:		
Time of primary minimum (HJD)	T_0	2 453 648.2848 (0.0002)
Secondary surface temperature (K)	$T_{\rm eff2}$	8600 (260)
Primary light contribution in the *U* band	$L_1/L_{1+2}(U)$	0.506 (0.010)
Primary light contribution in the *B* band	$L_1/L_{1+2}(B)$	0.497 (0.007)
Primary light contribution in the *V* band	$L_1/L_{1+2}(V)$	0.496 (0.005)
Primary light contribution in the *R* band	$L_1/L_{1+2}(R)$	0.504 (0.003)
Primary light contribution in the *I* band	$L_1/L_{1+2}(I)$	0.499 (0.005)
Surface potentials	$\Omega_{1,2}$	10.56 (0.23), 10.51 (0.25)
Mean relative radii	$r_{1,2}$	0.104 (0.002), 0.106 (0.002)
Orbital inclination (°)	i	85.8 (0.1)
Mass ratio	q	1.000 (0.002)
Semi-major axis ($R_\odot$)	a	16.76 (0.14)
Orbital eccentricity	e	0.0 (0.14)
Systemic velocity (km s^{-1})	V_γ	0.0 (0.4)
Fixed parameters:		
Orbital period (days)	P	4.077304
Albedo	$A_{1,2}$	1.0
Gravity-darkening exponent	$\tau_{1,2}$	1.0
Primary surface temperature (K)	$T_{\rm eff1}$	8600
Linear limb-darkening coefficient for *U*, *B*, *V*, *R*, *I*	x_1	0.640, 0.750, 0.645, 0.522, 0.419
Linear limb-darkening coefficient for *U*, *B*, *V*, *R*, *I*	y_1	0.243, 0.319, 0.282, 0.241, 0.209
Non-linear limb-darkening coefficient for *U*, *B*, *V*, *R*, *I*	x_2	0.641, 0.750, 0.645, 0.522, 0.410
Non-linear limb-darkening coefficient for *U*, *B*, *V*, *R*, *I*	y_2	0.243, 0.319, 0.282, 0.241, 0.209
Rotation rate	$F_{1,2}$	1.0
Chi-square for *UBVRI* light curves	$\chi^2_{\rm min}$	0.108, 0.016, 0.033, 0.013, 0.018

presented in Figure 2. All spectra observed around the H_α region are also shown together with orbital phases in Figure 3 in order to show the phase distribution of the observed spectrum and Doppler shifts of the component stars during the orbital motion. The journal of observations including observing times, mean signal-to-noise ratios (S/N) at 650 nm and exposure times is given in Table 3.

3 SPECTROSCOPIC ORBIT SOLUTION

Relatively sharp spectral lines (see Figure 2) of GSC 4019 3345 may allow a direct measurement of RVs by the Gaussian fitting to the line profiles. However, for most of the spectra of low S/N (see Table 3), weak lines become less reliable for RV measurements. Therefore, we avoided using cross-correlation or line-fitting techniques, but preferred to use a spectral disentangling method, the code KOREL (Hadrava, 1995), which is able to use all spectral information in spectral regions selected. Using the light contributions of the components, KOREL solves the pure Keplerian orbit, excluding eclipse effects on RVs, the so-called Rossiter–McLaughlin effect, and measures the RVs simultaneously. Additionally, it gives the disentangled spectrum of the component stars if the light contribution at the observed phases is provided correctly. In this study, the light contributions of the components are taken from the light-curve solution (Section 4), which are almost same for both components at out-of-eclipse phases except during the eclipses where the light contribution of the eclipsed component diminishes.

Since KOREL accepts input spectrum with 2^n data points, our spectra had to be re-binned. Therefore, we re-sampled our spectra to have 1 024 data points so that each pixel corresponded to $\sim$26 km s^{-1}. The orbital period is adopted from Equation (1) and kept fixed, while the time of periastron passage T_0, orbital eccentricity e, longitude of periastron w, and velocity semi-amplitudes $K_{1,2}$ have been converged during the orbital solution. The orbital solution yielded a small eccentricity ($e = 0.03$). The systemic velocity V_γ is measured by cross-correlating the spectrum at the time of conjunctions ($\phi = 0.497, 0.503$), with the RV standard star Vega (α Lyrae) as template. The final RVs are given in Table 3 and adopted orbital parameters with their uncertainties are given in Table 4. The best-fitting reconstructed spectra, together with observed one at two particular orbital phases ($\phi = 0.60, 0.70$), and the Keplerian orbital model are shown in Figure 4.

4 SIMULTANEOUS SOLUTION OF LIGHT AND RADIAL VELOCITY CURVES

The whole set of photometric data for LC analysis consists of 442 measurements in the *U* band, 578 in the *B* band, 890 in the *V* band, 572 in the *R* band, and 574 data points in the

Table 6. Close binary stellar parameters of GSC 4019 3345. Errors are given in parentheses.

Parameter	Symbol	Primary	Secondary
Spectral type	Sp	A4 V	A4 V
Mass ($M_\odot$)	M	1.92 (0.01)	1.92 (0.01)
Radius ($R_\odot$)	R	1.76 (0.05)	1.76 (0.05)
Separation ($R_\odot$)	a	16.76 (0.14)	
Orbital period (days)	P	4.0773040 (0.0000003)	
Orbital inclination (°)	i	85.8 (0.1)	
Mass ratio	q	1.000 (0.002)	
Eccentricity	e	0.0	
Surface gravity (cgs)	$\log g$	4.227 (0.011)	4.227 (0.014)
Integrated visual magnitude (mag)	V	12.15 (0.02)	
Integrated color index (mag)	$B-V$	0.40 (0.10)	
Intrinsic color index (mag)	$(B-V)_0$	0.12 (0.10)	
Color excess (mag)	$E(B-V)$	0.28 (0.10)	
Visual absorption (mag)	A_v	0.88 (0.10)	
Individual visual magnitudes (mag)	V	12.02 (0.05)	
Temperature (K)	$T_{\rm eff}$	8 600 (310)	8 600 (570)
Luminosity ($L_\odot$)	$\log L$	1.19 (0.09)	1.19 (0.14)
Bolometric magnitude (mag)	$M_{\rm bol}$	1.78 (0.18)	1.78 (0.22)
Absolute visual magnitude (mag)	M_v	1.79 (0.22)	1.79 (0.35)
Bolometric correction (mag)	BC	−0.01 (0.04)	−0.01 (0.04)
Velocity amplitudes (km s^{-1})	$K_{1,2}$	104.0 (0.1)	104.1 (0.1)
Systemic velocity (km s^{-1})	V_γ	−0.8(1.3)	
Computed synchronization velocities (km s^{-1})	$V_{\rm synch}$	22 (1)	22 (1)
Observed rotational velocities (km s^{-1})	$V_{\rm rot}$	70 (20)	70 (20)
Distance (pc)	d	1 104 (64)	
Age (Myr)	t	280 (40)	
Orbital angular momentum (cgs)	J_1, J_2	2.326 (13)$x10^{52}$, 2.329 (22)$x10^{52}$	
Proper motion (mas yr^{-1})	$\mu_\alpha \cos\delta, \mu_\delta$	−2.8 (4.1), −3.6 (4.1)	
Space velocities (km s^{-1})	U, V, W	15 (19), 8 (11), −17 (22)	

I band. The relatively low number of U-band data is due to the tracking errors of the telescope in long exposures during the U-band observations. The relatively high number of V-band data is due to the existence of extra V-band observations covering 2004–2007 observing seasons.

The catalog of the 2MASS survey gives the infrared magnitudes of GSC 4019 3345 as $J = 11.139 \pm 0.024$, $H = 11.040 \pm 0.026$, and $K = 11.001 \pm 0.020$, which yields the system color $J - H = 0.099 \pm 0.050$, implying a spectral type of A4–A5V (Covey et al. 2007). Since both components in the light curve have the same color, we can use the system color as the temperature indication for the component stars. Following temperature–spectral-type calibration tables of Straižys & Kuriliene (1981), we adopted a temperature of 8 600 K as an input temperature for the primary during the simultaneous analysis of LCs and RV data. The solutions have been carried out using the W-D program (Wilson & Devinney 1971; Wilson 1979, 1990). Eclipse effects in the RVs are taken into account during the solution. The logarithmic bolometric and monochromatic limb-darkening coefficients were interpolated from van Hamme's (1993) tables. In the gravity-darkening law ($T \sim g^{(\tau/4)}$), the gravity-darkening exponent τ was taken to be 1.0 for each component, which corresponds to $\beta = \tau/4 = 0.25$, as suggested by Lucy (1967) for early-type non-convective stars. A bolometric albedo was also set to 1.0 as suggested by Ruciński (1973) for early-type non-convective stars. Both fixed and adjusted parameters during the solutions are presented in Table 5.

The W-D program yielded a unique detached system with two equal components within the uncertainty box of output parameters. Table 5 lists the output parameters with their uncertainties. Figure 5 shows the best-fitting LC and RV models together with the observations.

5 DISCUSSION AND CONCLUSIONS

5.1 Close binary astrophysical parameters

Using the parameters of Table 5, which lists the results of simultaneous solutions of light and RV curves, fundamental astrophysical parameters of GSC 4019 3345 were computed and are listed in Table 6. Velocity semi-amplitudes of component stars in Table 6 are derived from the theoretical RV curve of simultaneous WD solutions, which are 1 km s^{-1} smaller than given in Table 4. The temperature $T_{\rm eff1} = 8\,600$ K, mass $M_1 = 1.92\,M_\odot$, and radii $R_1 = 1.77\ R_\odot$ of the components correspond to a spectral type of A4 in the main sequence (MS; e.g. Straižys & Kuriliene 1981). This result is in very good agreement with the infrared colors of the system (Section 4).

To obtain the space velocity of the system, we used the center-of-mass velocity, distance, and proper-motion values

of the system, which are given in Table 6. The proper-motion data were taken from the Tycho-2 Catalogue (Høg et al. 2000). The system's space velocity components (U, V, W), which are given with their errors in Table 6, were calculated using Johnson & Soderblom's (1987) algorithm.

5.2 Distance

Determination of the spectral types for the component stars allows us to interpret their intrinsic colors. Following the spectral type–intrinsic color calibration tables of Fitzgerald (1970), the intrinsic color of the system is adopted to be $(B - V)_0 = 0.12$ mag. Hence, using the observed color of $B - V = 0.40$, the color excess is found to be $E(B - V) = 0.28$ mag, which yields the visual absorption in the direction of GSC4019 3345 to be $A_v = 3.1 \times E(B - V) = 0.88$ mag. The unreddened Johnson V magnitude ($V_0 = V - A_v = 11.27$ mag) of GSC 4019 3345, when combined with the light contributions as derived from the light-curve analysis, yields the intrinsic V magnitudes of the component stars, $m_{V12} = 12.02$ mag. Using $M_v = 4.75$ mag as the absolute visual magnitude of the Sun and bolometric corrections $BC_{12} = -0.01$ mag for the primary and the secondary, from Straižys & Kuriliene (1981), bolometric and absolute visual magnitudes of the close binary components are derived (see Table 6). The visual magnitude and distance modulus indicate a photometric distance of 1 104 ± 64 pc to GSC 4019 3345.

5.3 Evolutionary scenario

The evolutionary status of GSC 4019 3345 has been investigated in the planes of log $T_{\rm eff}$–log L and log $T_{\rm eff}$–log g (Figure 6), using the latest evolutionary models and isochrones of Girardi et al. (2000; for the MS) and Siess et al. (2000; for the pre-main sequence, PMS), which include mass loss and moderate overshooting. As can be seen from Figure 6, the MS evolutionary tracks calculated for the components' mass ($M_{1,2} = 1.92$ M$_\odot$) show that both stars are in very early stages of their main-sequence lifetime. Different metal abundances imply different ages. Therefore, we have calculated three isochrones with a very low ($Z = 0.0001$, $Y = 0.23$), a solar, and a higher ($Z = 0.040$, $Y = 0.40$) metal abundance. The isochrones generated for the solar metal content imply a mean age of 280 ± 40 Myr for the system. The 6.3 Myr and 4 Gyr ages are indicated by the isochrones of higher and lower metal abundances.

In the case of detached binary systems, non-synchronous rotation can be used as an indicator for young age of the system. In order to find the rotation velocity of the components, the Mg II 4 481 Å line in the disentangled spectrum was modeled with the synthetic spectrum calculated using the Local Thermodynamic Equilibrium (LTE) Kurucz (1993) atmosphere models, with new opacity distribution functions provided by Castelli & Cacciari (2001). The synthetic model calculation was achieved with the SYNTHE routine (Kurucz 1993). Solar metal abundance and a microturbulence velocity

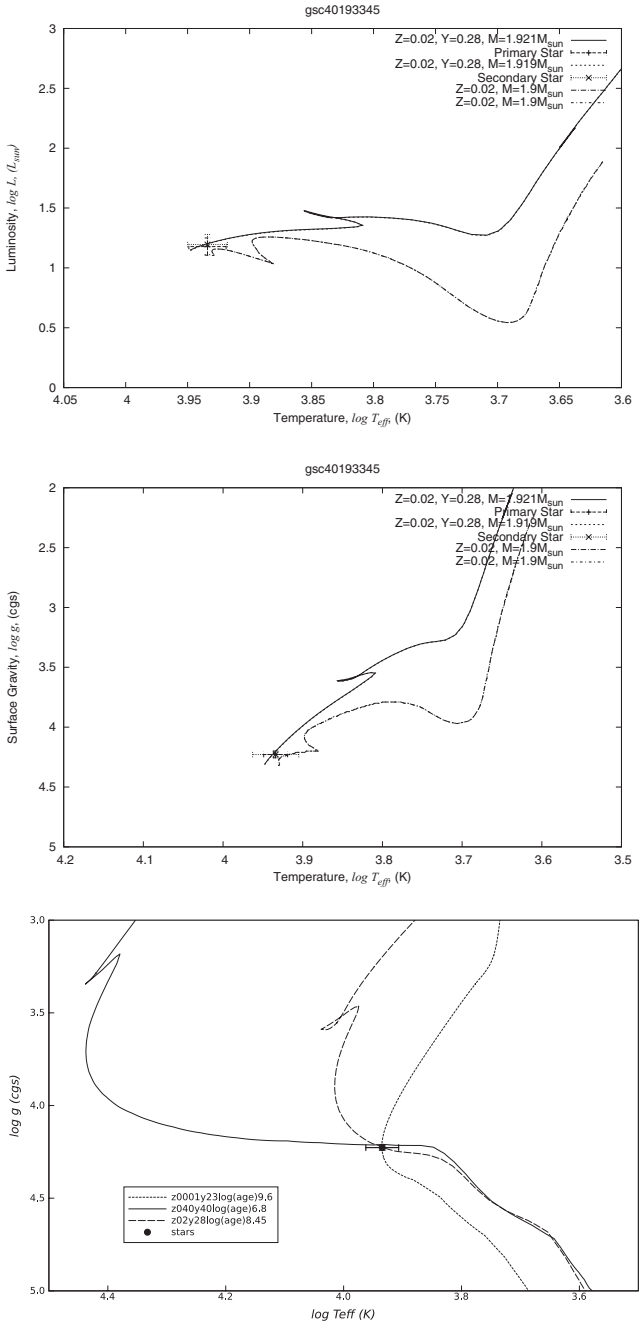

Figure 6. Evolutionary tracks in the log $T_{\rm eff}$–log L (top) and log $T_{\rm eff}$–log g (middle) planes. In the top and middle panels, solid and dashed lines are the evolutionary tracks for MS and PMS stages, respectively. MS evolutionary tracks for the exact masses of the components are indistinguishable. The PMS evolutionary tracks are calculated for $M = 1.9\,M_\odot$. Isochrones generated with different metallicities in the log $T_{\rm eff}$–log g plane (bottom).

of 2 km s^{-1} were assumed in the model atmosphere calculations. The instrumental broadening of TFOSC was estimated to be 40 km s^{-1} from Fe–Ar lines.

The best-fitting model atmosphere revealed the atmosphere parameters as $T_{\rm eff} = 8\,500 \pm 300$ K, log $g = 4.25 \pm 0.25$ cgs, and $V_{\rm rot} \sin i = 70 \pm 20$ km s^{-1}. The synthetic Mg II 4 481 Å line produced according to the model atmosphere

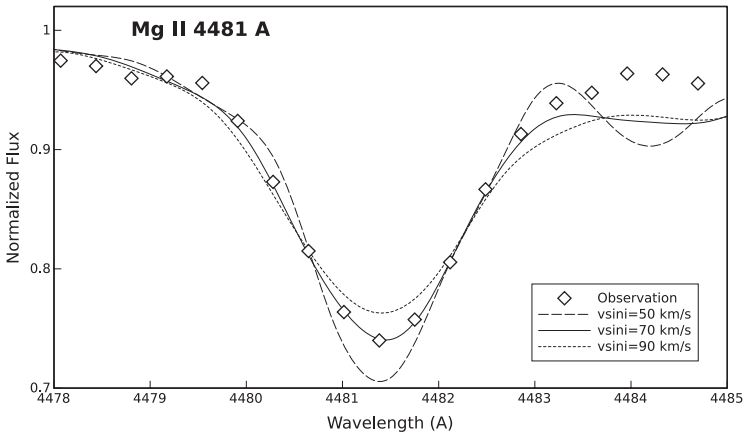

Figure 7. Synthetic spectra calculated with various projected rotational velocities fitted on the disentangled Mg II 4 481 Å line.

well fitted to the component spectra (Figure 7). The effective temperature used in model atmosphere fitting is found to be in good agreement with the temperature used in the LC analysis, and the observed rotation velocities of the components ($V_{\rm rot} = 70$ km s^{-1}) are about three times higher than the computed ones ($V_{\rm synch} = 22$ km s^{-1}), which imply a very young age for the system that did not yet have the time to synchronize their rotations with the orbit.

6 CONCLUDING REMARKS

1. There were only three A-type twins known among the binary systems with reliable spectroscopic data. Early-type (OBA) twins have great importance since their formation scenario is not very well known as of low-mass twins of F, G, and K spectral types. The precise physical parameters derived for GSC 4019 3345 in this study increased the number of early-type known twins to four.

2. Both components of GSC 4019 3345 occupy the same location on the Hertzsprung-Russell (H-R) diagram according to the derived luminosity, effective temperature, and surface gravity values. Hence, evolutionary status (ages) is similar for both components. This means that both components of GSC 4019 3345 passed the mass accretion phase during the formation at the same time within the derived parameters' uncertainty boxes. On the contrary, it is not possible with present accuracy to prove or disprove that GSC 4019 3345 contradicts with Parenago 1802, the low-mass binary with an age difference between the components (e.g. Stassun et al. 2008), since the age difference between the components of Parenago 1802 is on the order of several hundred thousand years that is beyond the accuracy of the present study.

3. The synchronization time scale for the component stars of GSC 4019 3345 is, following Zahn (1977), on the order of 3 Myr. Nevertheless, the orbital circularization time scale is, again following Zahn (1977), on the order of 570 Myr. The age of GSC 4019 3345 is clearly higher than the synchronization time scale but lower than the circularization time scale of the system. According to the estimated system age, the system should have been in a non-circular orbit with a pseudosynchronized rotation. Supersynchronism itself is unusual for a binary with circular orbit since tidal synchronization proceeds faster than tidal circularization. However, such unusual supersynchronism is also found in the M35 open cluster ($\tau = 150$ Myr) in a binary ($P_{\rm orb} = 10.3$ days) having circular orbit with four times supersynchronous rotation (Meibom et al. 2006). Obviously, such systems are challenges for the present tidal evolution theory.

Higher resolution spectroscopy of the system is strongly needed to study the spectral lines in the individual spectrum of the components. This will enable one to know the metal content of the components, which will provide more reliable age estimates for GSC 4019 3345.

ACKNOWLEDGMENTS

Photometric observations are granted by the Çanakkale Onsekiz Mart University Observatory. Spectroscopic observations are granted by the TUBITAK National Observatory with the project code 11BRTT150-202-0. We thank Drs Afşar Kabaş and Naci Erkan for their help during the photometric observations. We thank the referee for useful comments that contributed to the scientific improvement of the manuscript.

REFERENCES

Bakış, V., Bakış, H., Demircan, O., Erdem, A., & Cicek, C. 2007, ASPC, 370, 251
Castelli, F., & Cacciari, C. 2001, A&A, 380, 630
Covey, K. R., et al. 2007, AJ, 134, 2398
Fitzgerald, M. P. 1970, A&A, 4, 234
Girardi, L., Bressan, A., Bertelli, G., & Chiosi, C., 2000, A&AS, 141, 371
Hadrava, P. 1995, A&AS, 114, 393
Høg, E., et al. 2000, A&A, 355, 27
Johnson, D. R. H., & Soderblom, D. R. 1987, AJ, 93, 864
Kurucz, R. L. 1993, CD-ROM 13, 18 (http://kurucz.harvard.edu)

Kwee, K. K., & van Woerden, H. 1956, BAN, 12, 327
Lucy, L. B. 1967, ZA, 65, 89
Lucy, L. B. 2006, A&A, 457, 629
Meibom, S., Mathieu, R. D., & Stassun, K. G. 2006, ApJ, 653, 621
Monet, D., Canzian, B., Harris, H., Reid, N., Rhodes, A., & Sell, S. 1997, A Catalog of Astrometric Standards, US Naval Observatory Flagstaff Station
Ruciński, S. M. 1973, AcA, 23, 79.
Siess, L., Dufour, E., & Forestini, M. 2000, A&A, 358, 593
Simon, M., & Obbie, R. C. 2009, AJ, 137, 3442
Stassun, K. G., Mathieu, R. D., Cargile, P. A., Aarnio, A. N., Stempels, E., & Geller, A. 2008, Natur, 453, 1079
Straižys, V., & Kuriliene, G. 1981, Ap&SS, 80, 353
van Hamme, W. 1993, AJ, 106, 2096
Wilson, R. E. 1979, ApJ, 234, 1054
Wilson, R. E. 1990, ApJ, 356, 613
Wilson, R. E., & Devinney, E. J. 1971, ApJ, 166, 605
Zahn, J. P. 1977, A&A, 57, 383
Zinnecker, H., & Yorke, H. W. 2007, ARA&A, 45, 481